

This manuscript entitled “A machine learning approach for ozone forecasting and its application for Kennewick, WA” is a preprint and will be submitted for publication in **Environmental Science and Technology** and then undergo the peer-review process. If accepted, the final version of this manuscript will be available via the ‘Peer-reviewed Publication DOI’ link on the right-hand side of this webpage. Please feel free to contact any of the authors and we welcome feedback. The authors and affiliations of the manuscript are:

Kai Fan

Laboratory for Atmospheric Research, Civil and Environmental Engineering, Washington State University

kai.fan@wsu.edu

Brian Lamb

Laboratory for Atmospheric Research, Civil and Environmental Engineering, Washington State University

blamb@wsu.edu

Ranil Dhammapala

Washington State Department of Ecology

ranil.dhammapala@ecy.wa.gov

Ryan Lamastro

State University of New York at New Paltz

lamastrr1@hawkmail.newpaltz.edu

Yunha Lee

Laboratory for Atmospheric Research, Civil and Environmental Engineering, Washington State University

yunha.lee@wsu.edu

1 A machine learning approach for ozone forecasting
2 and its application for Kennewick, WA

3 *Kai Fan¹, Ranil Dhammapala², Ryan Lamastro³, Brian Lamb¹, and Yunha Lee¹*

4 *¹Laboratory for Atmospheric Research, Civil and Environmental Engineering, Washington State*
5 *University*

6 *²Washington State Department of Ecology*

7 *³State University of New York at New Paltz*

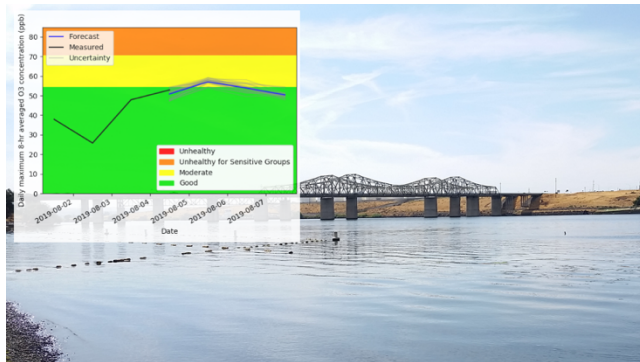
8 *Corresponding Author

9 E-mail: yunha.lee@wsu.edu (Yunha Lee)

10
11 **ABSTRACT:**

12 Chemical transport models (CTM) are widely used for air quality modeling, but these models miss
13 forecasting some air pollution events, and require a lot of computational power. In Kennewick,
14 WA, elevated O₃ episodes can occur during the summer and early fall, but the CTM-based
15 operational forecasting system (AIRPACT) struggles to capture them. This research used the 2015
16 – 2018 historical archives from the Weather Research and Forecasting (WRF) meteorological
17 model forecasts produced daily by the University of Washington, and O₃ observation data at

18 Kennewick to train two machine learning modeling frameworks, ML1 and ML2 for a reliable
19 forecasting system. ML1 used the random forest (RF) classifier and multiple linear regression
20 (MLR) models, and ML2 used a two-phase RF regression model with best-fit weighting factors.
21 Since April 2019, the ML modeling frameworks have been used to produce daily 72-hour O₃
22 forecasts and have provided the forecasts via the web for the agency and public use. For the peak
23 O₃ days, AIRPACT showed a large variation, while ML2 underpredicted and ML1 performed the
24 best. In the future, this dual ML forecast system will be applied to other locations within the Pacific
25 Northwest.



26

27 1. INTRODUCTION

28 Chemical transport models (CTM) are widely used to simulate the temporal and spatial variation
29 of air quality.¹ CTMs include various atmospheric physical and chemical processes as well as
30 sources and sinks. However, not every physical and chemical process in the atmosphere has been
31 understood.² Even though the accuracy of numerical models keeps improving, there are still large
32 uncertainties and errors in the simulations. For the CTMs, the high computational cost is an
33 additional concern.

34 The Air Indicator Report for Public Awareness and Community Tracking (AIRPACT) was
35 developed for air quality forecasting in the Pacific Northwest in the U.S. AIRPACT uses the
36 Community Multiscale Air Quality Modeling System (CMAQ) model to compute air quality with
37 the Weather Research and Forecasting (WRF) meteorology. The AIRPACT domain mainly covers
38 Washington, Idaho and Oregon State with 4 km horizontal grid cells and 37 vertical levels. The
39 hourly simulations use the Carbon Bond, version 5 (CB05) as the gas chemistry mechanism and
40 AERO6 as the aerosol module. AIRPACT 48-hour forecasts are produced daily and provided via
41 the web to the public and local air quality agencies (<http://lar.wsu.edu/airpact/>).

42 Within the AIRPACT domain, Kennewick is part of the Tri-cities metropolitan area with a total
43 population of about 216,000 (Estimated population of Kennewick 83,670, Pasco 75,290 and
44 Richland 56,850 in 2019).³ The city is 32 km north of Washington State's southern border and is
45 in a hot dry portion of the state. Recent monitoring and a large field study have shown that a few
46 high O₃ events typically occur during summer and early fall.⁴ While AIRPACT forecasts initially
47 predicted the Tri-cities area as an ozone hotspot, the daily forecasts struggle to forecast correctly
48 high O₃ concentrations in this area. There were 20 days when the air quality was unhealthy for
49 sensitive groups in 2015 – 2018, but AIRPACT only captured one of them.

50 Machine learning (ML) models have been used to predict air quality in recent years. These
51 methods incorporate a variety of features, including observed pollutant levels and various
52 meteorological variables as the basis for training and applying ML methods. For example, Feng
53 et al.⁵ input trajectory-based geographic parameters, meteorological forecasts and associated
54 pollutant predictors to an artificial neural network to predict PM_{2.5} concentrations in Beijing,
55 China. Freeman et al.⁶ used a recurrent neural network with short-term memory to predict 72-hour
56 O₃ forecasting with training via hourly air quality and meteorological data. Zamani Joharestani et

57 al.⁷ tested three machine learning approaches, random forest, extreme gradient boosting and deep
58 learning to predict the PM_{2.5} concentrations in Tehran, Iran using 23 features.

59 A successful ML model must be trained with a large dataset. For air quality prediction, the
60 training dataset usually includes meteorological data (temperature, relative humidity, pressure,
61 wind speed and direction, etc.) and observed pollutant concentrations. However, compared to
62 numerical models, ML methods tend to be more computationally efficient, require less input data,
63 and perform better for specific events, which makes ML models popular in recent years.^{5,6,8-10}

64 In this study, we developed ML modeling frameworks to predict O₃ mixing ratios, which were
65 based on the following approaches: random forest (RF) and multiple linear regression (MLR). RF
66 is one of the most popular machine learning methods and has been used in many air quality
67 modeling and forecast studies. The RF method has been demonstrated to provide reliable forecasts
68 for O₃ and PM_{2.5} with lower computational cost compared to physical models.¹¹⁻¹⁴ RF consists of
69 an ensemble of decision trees, and decision tree learning is for approximating discrete-valued
70 functions.¹⁵⁻¹⁷ The RF model can be used for classification and regression. For our study, the RF
71 classifier model was used to predict the O₃ Air Quality Index (AQI) categories, and the RF
72 regression model was used to predict O₃ mixing ratios. MLR is a regression method with one
73 dependent variable and several independent variables, which we used to predict O₃ levels.
74 Previous studies that used MLR models to predict O₃ mixing ratios showed performance as good
75 as more complex machine learning models.¹⁸⁻²¹ Yuchi et al.²² used RF and MLR for indoor air
76 quality forecasts, and RF showed better in-sample predictions, MLR showed better out-of-sample
77 predictions. So, this paper will discuss the application of both RF and MLR for O₃ forecasts.

78 The goal of this study was to provide reliable air quality forecasts using machine learning
79 approaches, especially for high O₃ events in Kennewick, WA. Section 2 presents the two machine

80 learning modeling frameworks we developed, including the training dataset. Section 3 presents the
81 feature selection, evaluation of the model performance using 10-time 10-fold/walk-forward cross-
82 validation and a summary of the forecast results in 2019.

83

84 **2. DATASETS AND MODELING FRAMEWORKS**

85 **2.1. Training dataset.**

86 The training dataset for our machine learning models includes the previous day's observed O₃
87 mixing ratios, time information (hour, weekday, month), and simulated meteorology from daily
88 WRF forecasts from May to September in 2015 – 2018 at Kennewick, WA. Because the heat and
89 sunlight favor the O₃ generation,²³ and wildfires can generate the O₃ precursors,²⁴ observations are
90 only made from May to September. The training dataset covered this period. The WRF
91 meteorology was obtained from the University of Washington,^{25,26} which is used in AIRPACT as
92 an input to generate emissions and air quality forecasting. We used the temperature, surface
93 pressure, relative humidity, wind speed, wind direction, and planetary boundary layer height (PBL)
94 in the training dataset. Time information was included in the training dataset due to the significant
95 trend of O₃ variation in the diurnal, weekday and monthly scales. Table S1 summarizes the
96 historical O₃ AQI during the training period. Here we define a high O₃ day as the day when the
97 observed AQI category is worse than Moderate (i.e. AQI category 3 or worse). The high O₃ days
98 in all the years used here are less than 5% of total simulated days, except for 2017. Extensive
99 wildfires occurred in 2017, and there were 8 days that the air quality was unhealthy for sensitive
100 groups (i.e., O₃ AQI category = 3). The days when the wildfire smoke caused excess O₃ were
101 marked in the historical data, but it could not be involved in the training dataset because it was not

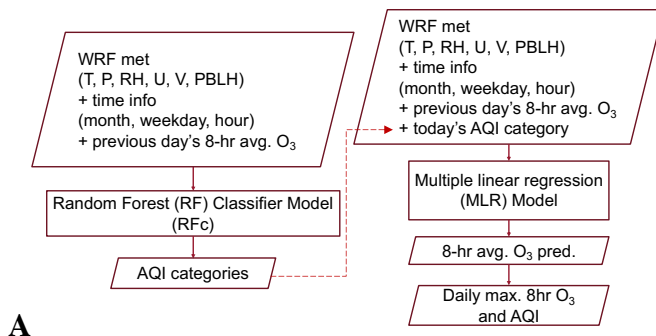
102 predictable. And there were only four days in this case, so it would not affect the model training
103 significantly.

104

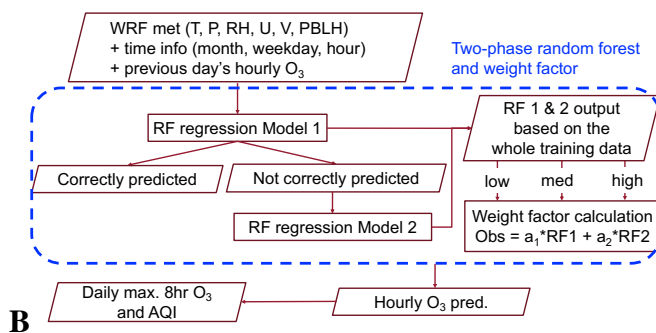
105 **2.2. Machine learning modeling frameworks**

106 We have developed two O₃ forecast modeling frameworks based on ML methods. The first
107 machine learning modeling framework (ML1, hereafter; see Figure 1A) used RF classifier and
108 MLR models. The *RandomForestClassifier* and *RFE* functions in the python module *sklearn* were
109 used. In ML1, the WRF meteorology, time information, and previous day's 8-hour averaged O₃
110 mixing ratios were first used to train an RF classifier model to predict AQI categories. There are
111 not many high O₃ cases, which makes the dataset imbalanced, and the imbalanced training data
112 may lead the bias toward the low O₃ prediction.²⁷ To address the problem from the imbalanced
113 data, the *balanced_subsample* option was turned on for the RF classifier. The *balanced_subsample*
114 gives weights to the AQI category values based on their frequency in the bootstrap sample for each
115 tree, so the high AQI values with low frequency in the training dataset are weighted proportionally
116 more. Separately, the observed AQI categories were added to the training dataset to train the MLR
117 model. When used for forecasting, the RF classifier model was first used to predict the AQI
118 categories, which were in turn fed into the MLR model to predict the O₃ mixing ratios, as the red
119 dashed line shown in Figure 1A.

120



121



122 **Figure 1.** (A) ML1 modeling framework based on random forest (RF) classifier and multiple linear
 123 regression (MLR) models (B) ML2 based on a two-phase RF regression and weight factors

124

125 Machine Learning modeling framework 2 (ML2 hereafter; see Figure 1B) is based on a two-
 126 phase random forest regression model. The *RandomForestRegressor* function in the python
 127 module *sklearn* was used. ML2 used the WRF meteorology, time information, and previous day's
 128 hourly O₃ mixing ratios to train an RF regression model to predict O₃ mixing ratios. The whole
 129 historical dataset was used to train the first RF regression model (RF1 in Figure 1B). The training
 130 data was isolated when RF1 predicted O₃ mixing ratios differed from the observations by more
 131 than 5 ppb, and then the isolated dataset was used to train the second RF regression model (RF2
 132 in Figure 1B). The training dataset for RF2 was a subset of the whole training data, so RF2 required
 133 more decision trees (100 trees for RF1 and 200 trees for RF2).²⁸ This is why it is called a two-

134 phase RF regression model. The RF1 predicted O₃ mixing ratios were divided into three levels
135 (low: < 30 ppb, medium: 30 – 50 ppb, high: > 50 ppb). For the data within each level, a set of
136 weighting factors, a₁ and a₂, were computed based on a linear regression equation,

$$137 \quad O_{3\text{observed}} = a_1 * RF_1 + a_2 * RF_2 \quad (1)$$

138 When doing forecasting, RF1 and RF2 were used to provide initial predictions. The RF1
139 prediction determined which weighting factors would be used. The hourly O₃ prediction was
140 computed as

$$141 \quad O_3 = a_1 * RF_1 + a_2 * RF_2 \quad (2)$$

142

143 **2.3. Ensemble forecasting system**

144 The ML1 and ML2 modeling frameworks have been used to provide 72-hour “ensemble”
145 operational O₃ forecasts each day, by using more than 20 members from the
146 University of Washington Mesoscale Ensemble system (<https://a.atmos.washington.edu/wrft/ensembles/info.html>) beginning in April 2019. We predicted the O₃ levels with each WRF member to
147 compile a 72-hour ensemble mean forecast with an associated uncertainty range. The forecasts are
148 available to the public on <http://ozonematters.com>, with the ability to sign up for email alerts if
149 “Unhealthy for Sensitive Groups” or worse levels are forecast. To increase the size of the training
150 dataset and improve the forecast accuracy, we included the new observational data from the
151 previous day and re-trained the models daily. For the ensemble daily forecasts, the computational
152 time is approximately 1 min for ML1 and less than 3 min for ML2.

154

155 **2.4. Statistical methods for O₃ AQI evaluation**

156 Two parameters, Heidke Skill Score (HSS) and the Hanssen-Kuiper Skill Score (KSS) were used
 157 to evaluate the machine learning model prediction. Table S2 is a 2x2 contingency table, which
 158 shows the simple yes or no cases.²⁹ For the air quality research, “yes” usually means air pollution
 159 events, and “no” means good air quality. The equations (3) and (4) show how HSS and KSS are
 160 computed.³⁰

161
$$HSS = \frac{a + d - a_r - d_r}{n - a_r - d_r} \quad (3)$$

162 Where $a_r = \frac{(a+b)(a+c)}{n}$, $d_r = \frac{(b+d)(c+d)}{n}$

163
$$KSS = \frac{ad - bc}{(b + d)(a + c)} \quad (4)$$

164 HSS represents the accuracy of the model prediction compared with a reference forecast (r in
 165 equation 3), which is from the random guess that is statistically independent of the observations.^{30,31}
 166 The range of the HSS is from $-\infty$ to 1. A negative value means a random guess is better, 0 means
 167 no skill, and 1 means a perfect score. KSS measures the ability to separate different categories.
 168 The range is from -1 to 1 where 0 means no skill, and 1 means a perfect score.

169 For the multi-category case in this research with AQI 1 (Good), 2 (Moderate) or 3 (Unhealthy
 170 for Sensitive Groups), we use the 3x3 contingency table in Table S3 ³². The skill scores are
 171 computed as follows.³⁰

172
$$HSS = \left(\sum_{i=1}^3 p_{ii} - \sum_{i=1}^3 p_i \hat{p}_i \right) / \left(1 - \sum_{i=1}^3 p_i \hat{p}_i \right) \quad (5)$$

173
$$KSS = \left(\sum_{i=1}^3 p_{ii} - \sum_{i=1}^3 p_i \hat{p}_i \right) / \left(1 - \sum_{i=1}^3 p_i p_i \right) \quad (6)$$

174 The p_{ii} is the sample frequency when the observed and model predicted AQI is i , and p_i and \hat{p}_i
175 are the observed and model predicted sample frequency when AQI = i . The multi-category case is
176 based on the simple yes or no case, and the skill scores, HSS and KSS have the same meaning as
177 the simple case.

178

179 **3. RESULTS AND DISCUSSION**

180 **3.1. Feature selection for machine learning models**

181 There were 10 features for the RF classifier and regression model and 11 features for the MLR
182 model. Too many features can cause an overfitting problem,³³ so the attributes
183 *feature_importances_* in function *RandomForestClassifier/RandomForestRegressor* and *ranking_*
184 in *RFE* were used to do the feature selection. The selected features were input to train the model.

185 There were two components in ML1, RF classifier and MLR model. For an RF model, the feature
186 selection function with the default setting computed the importance weights, and the features
187 whose weight was above the mean weight were selected. The feature weights could change in each
188 training process, but the ranking showed very little variation. The previous day O₃ observation,
189 temperature and hour were the primary features selected, and the relative humidity was selected in
190 some cases. The default number of selected features for MLR was half of the total features
191 available, so two more features were chosen by the built-in feature selection function, in addition
192 to the three primary features: the previous day O₃ observation, temperature, relative humidity, AQI
193 category, and surface pressure. The output of each framework was hourly O₃ mixing ratios for

194 each 72-hour forecast. For evaluation purposes, these forecast values were compiled into the
195 maximum daily 8-hour moving average O₃ (MDA8).

196 The feature selection function for RF regression was the same as the RF classifier model.
197 Temperature, previous O₃ observation, PBL height or relative humidity, were the selected features
198 for the first phase RF regression model, and the temperature and hour were selected for the second
199 phase.

200

201 **3.2. Machine learning model evaluation**

202 Cross-validation is commonly used for model evaluation, since it can test the subset of the dataset
203 with an equal chance.³⁴ There are various cross-validation methods, such as leave-one-out, k-fold,
204 etc. Here, the 10-time 10-fold and walk-forward cross-validation were used to evaluate the two
205 modeling frameworks. The input data were the primary WRF output, time information and
206 historical O₃ observations in Kennewick.

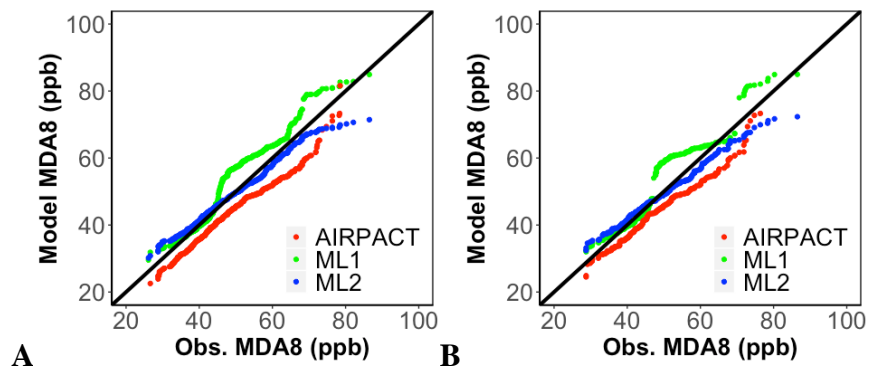
207

208 3.2.1 10-time 10-fold cross-validation

209 The k-fold cross-validation may be the most commonly used technique for the model evaluation.³⁴
210 It divides the dataset into k randomly chosen parts (k=10 in this research), and k-1 parts are used
211 to train the model, the remaining portion is used to test the model, and this process is repeated k
212 times to test all k subsets. The *RepeatedKfold* function in the python module *sklearn* was used to
213 separate the dataset. To avoid any bias from data separation, the k-fold cross-validation was
214 repeated 10 times in this research.

215 The NMB for these 10-time cross-validation was $6.3\% \pm 0.2\%$ for ML1 and $0 \pm 0.1\%$ for ML2.
216 The AIRPACT NMB was -9.3% , which was lower than ML1 and ML2. The standard deviations
217 show that there is no significant difference among each repeat, and the model performance is
218 stable.

219 The Q-Q plots in Figure 2A show the comparison between the model predictions and
220 observations. AIRPACT underpredicted the MDA8 for MDA8 lower than 70 ppb. For MDA8
221 higher than 70 ppb, AIRPACT tended to predict the DMA8 close to the 1:1 line, but there were
222 several extremely high predictions from AIRPACT which were not shown in Figure 2A. ML1 and
223 ML2 were close to the 1:1 line when the MDA8 was lower than 45 ppb. ML1 was close to the 1:1
224 line for MDA8 in the 60 – 70 ppb range. For high MDA8 cases (> 70 ppb), ML1 showed the best
225 performance.

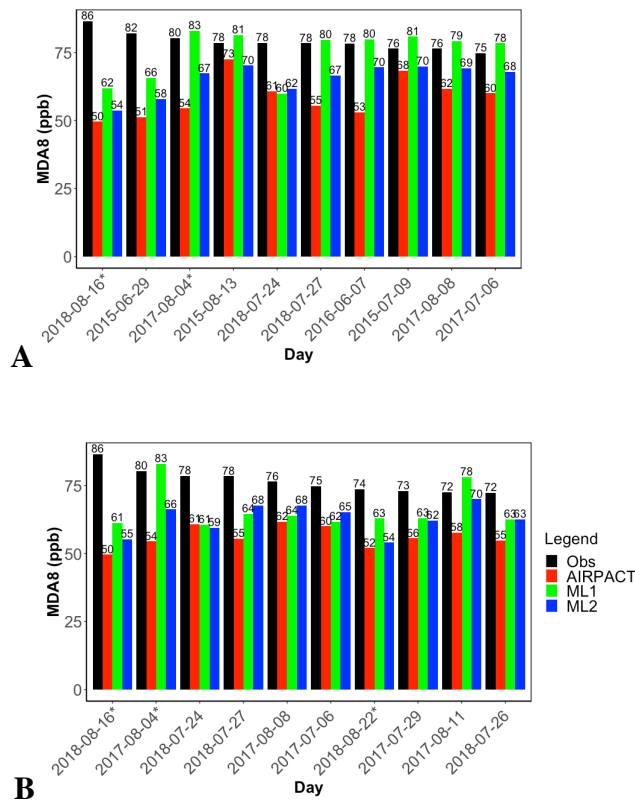


226 **Figure 2.** Q-Q plots of averaged model vs. observed MDA8 (A) during May – September 2015 –
227 2018 based on the 10 times 10-fold cross-validation (B) during May – September 2017 – 2018
228 based on the walk-forward cross-validation
229

230
231 The highest 10 observed MDA8 during 2015 – 2018 and their model predictions were selected
232 and shown in Figure 2B. ML2 and AIRPACT underpredicted all 10 cases, and ML1 provided

233 close predictions for 7 out of 10. These results show that ML1 performs better for high O₃ events,
 234 and results from the Q-Q plot also confirms this. The two ML models showed a similar trend,
 235 and they both largely underpredicted 3 cases. So, they may miss the same factor which led to the
 236 high MDA8. The highest O₃ day was affected by the wildfire smoke, and all models missed it.

237



238

239 **Figure 3.** Top 10 observed MDA8 and model predictions from (A) 10-time 10-fold cross-
 240 validation (B) the walk-forward cross-validation

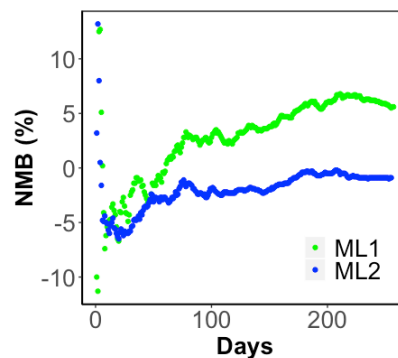
241 * means that the wildfire smoke caused excess ozone on that day

242

243 3.2.2 Walk-forward cross-validation

244 The 10-time 10-fold cross-validation does not consider the temporal order of the data,
245 which is important for the time-series data. Walk-forward cross-validation is a technique for time-
246 series data.³⁵ For this evaluation, the 2015 and 2016 data were used to train the model and predict
247 the first day in the 2017 dataset (May 1st, 2017). Then the May 1st, 2017 data was included in the
248 training dataset and the models were used to predict O₃ for May 2nd, 2017. This process was
249 repeated for each additional day of the 2017 and 2018 ozone seasons.

250 When a new day's MDA8 was predicted by the ML models, the NMB was recomputed by
251 including the new prediction. The change of NMB was shown in Figure 3A. In the beginning,
252 there was no clear trend for the NMB values for both ML models. The NMB from ML1 prediction
253 sharply increased after June 2017 (Day 50 in Figure 3A) when more high O₃ events occurred,
254 slowly increased after August 2017 (Day 100 in Figure 3A), and slowly decreased after July 2018
255 (Day 200 in Figure 3A). The overprediction from ML1 during the low O₃ periods (May and June)
256 could lead to the NMB increasing, while the NMB values were stable or even decreasing during
257 the high O₃ period (July and August). For ML2, there were some fluctuations before August 2018,
258 and the NMB was stable after that. For both ML1 and ML2, the NMB values were getting stable
259 when more data got involved. The final NMB of two ML models were 5.6% and -0.9%, which
260 were lower than the 10-time 10-fold cross-validation.



261
262 **Figure 4.** The walk-forward NMB of each time step for ML1 and ML2

263

264 The walk-forward cross-validation provided two-year MDA8 predictions (2017 and 2018), and
265 the Q-Q plots were similar to the 10-time 10-fold cross-validation. The two breakpoints of ML1
266 distribution were clearer in Figure 3B. Ten highest MDA8 in 2017 and 2018 were shown in Figure
267 4. ML1 only captures 2 out of the top 10 observed MDA8 and ML2 captured 1. In some cases,
268 ML1 was even lower than ML2. Three high O₃ days with stars (*) in Figure 4 were affected by the
269 wildfire smoke, and ML1 captured two of them. The two ML models still performed better than
270 AIRPACT.

271 Table 1 summarizes the HSS and KSS of the two machine learning models and AIRPACT from
272 the two cross-validation methods. Both machine learning models show better performance with
273 higher HSS and KSS values than AIRPACT. ML2 shows higher HSS than ML1 for both cross-
274 validation results, which means ML2's prediction is generally more accurate. ML1 shows higher
275 KSS in 10-time 10-fold cross-validation due to its better performance of high O₃ predictions. The
276 statistics from AIRPACT and ML2 are close between two cross-validations, but HSS and KSS
277 from walk-forward are lower than 10-time 10-fold cross-validation.

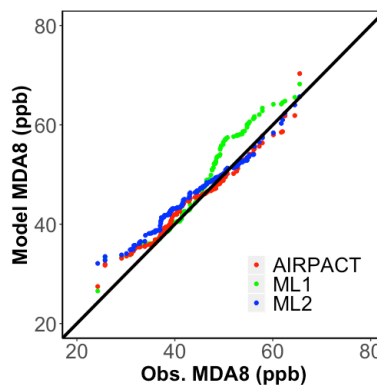
278 **Table 1. HSS and KSS from two cross-validations**

		AIRPACT	ML1	ML2
10-time 10-fold	HSS	0.32	0.44	0.55
	KSS	0.25	0.62	0.50
Walk-forward	HSS	0.34	0.37	0.57
	KSS	0.27	0.53	0.51

279

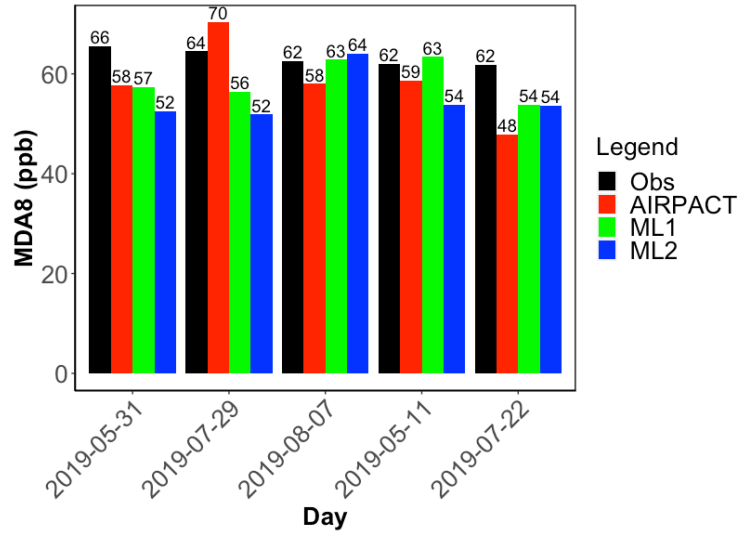
280 **3.3. O₃ ensemble forecasting in 2019**

281 Since April 2019, our machine learning models have been used for operational O₃ ensemble
282 forecasting for Kennewick, WA. The ensemble forecasting to predict O₃ levels was based on more
283 than 20 WRF ensemble members provided by the University of Washington. The difference
284 among the predicted MDA8 from the ensemble members was not significant (within 5%). To better
285 compare with the evaluation in the previous section, this section only covers the data from May to
286 September in 2019. The ML1 and ML2 results are the ensemble means of the MDA8 values from
287 more than 20 ML forecasts. The Q-Q plot in Figure 5 shows that the ML1, ML2 and AIRPACT
288 model forecasts are close for O₃ lower than 40 ppb. For the O₃ in 40 – 60 ppb, ML1 tends to
289 overpredict, while AIRPACT and ML2 are closer to observations. When the O₃ mixing ratio is
290 higher than 60 ppb, ML1 slightly overpredicts, ML2 underpredicts, and AIRPACT varies in cases.
291 For the highest 5 MDA8 points in Figure 6, the observed values were 62 – 66 ppb, while ML1’s
292 predictions were closer to the observations than AIRPACT and ML2. AIRPACT showed larger
293 variation (48 – 70 ppb) compared to two ML models.



294

295 **Figure 5.** Q-Q plots of ensemble mean model vs. observed MDA8 during May - September 2019

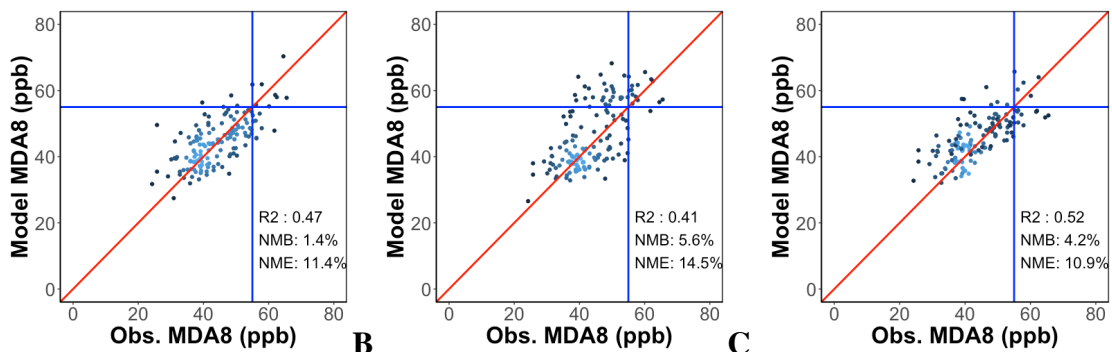


296

297 **Figure 6.** Top 5 observed MDA8 and model predictions in 2019

298

299 The scatter plots in Figure 7 show the ensemble mean MDA8 from May to September in 2019.
 300 ML2 shows relatively higher R^2 value (0.52) than ML1 (0.41) and AIRPACT (0.47). The NMB of
 301 AIRPACT is lowest (1.4%), but its NME (11.4%) is higher than ML2 (10.9%). The low NMB is
 302 due to the offset of overprediction and underprediction. ML1 tended to overpredict the MDA8 O_3
 303 especially when it was higher than 40 ppb. Because of mostly favorable meteorological conditions
 304 and few wildfires in the Pacific Northwest, the O_3 mixing ratios were not very high in 2019 and
 305 the model performance of ML2 was the best.



306

A

B

C

307 **Figure 7.** Scatter plots of observed vs. ensemble mean MDA8 of AIRPACT in (A), ML1 in (B)
 308 and ML2 in (C) at Kennewick from May to September in 2019

309

310 The model performance statistics are presented in Table 2, the blue cells show misses, and red
 311 cells show false alarms. In 2019, all the AQI_{obs} at Kennewick were less than 3. Compared to
 312 AIRPACT, ML1 captured high O_3 days better (15 events vs. 7 events for $AQI_{obs}2$) but tended to
 313 overpredict the O_3 AQI (26 false alarm events vs. 3 false alarm events). ML2 predicted similar
 314 AQI days to AIRPACT. Based on the analysis above, we decided to use ML1 to provide the daily
 315 forecasting for Kennewick when the predicted AQI was above 2, and ML2 when the predicted
 316 AQI was 1 or 2.

317 **Table 2. Number of days for each AQI during May – September 2019**

		Observation					
		AQI 1		AQI 2		AQI 1	
AQI 2	AQI 1	122	11	99	3	119	13
	AQI 2	3	7	26	15	6	5
		AIRPACT		ML1		ML2	

318 ML1 and ML2 are the ensemble mean results using 20 WRF ensemble members.

319 The blue cells mean the model misses high O_3 , and the red cells mean the model raises false
 320 alarms.

321

322 **Acknowledgement**

323 We thank the fund from CEE - YUNHA LEE ACCRUALS (2315-0028). We acknowledge that

324 David Ovens from University of Washington helped setup a data feed of WRF ensembles.

325 **Reference:**

- 326 (1) Sportisse, B. A Review of Current Issues in Air Pollution Modeling and Simulation.
327 *Computational Geosciences* **2007**, *11* (2), 159–181. <https://doi.org/10.1007/s10596-006-9036-4>.
- 328 (2) Seinfeld, J. H.; Pandis, S. N. *Atmospheric Chemistry and Physics: From Air Pollution to*
329 *Climate Change*; John Wiley & Sons, 2016.
- 330 (3) April 1, 2019 Population of Cities, Towns and Counties Used for Allocation of Selected
331 State Revenues State of Washington. Washington State Office of Financial Management 2019.
- 332 (4) B. T. Jobson; G. VanderSchelden. *The Tri-Cities Ozone Precursor Study (T-COPS)*; Final
333 Report; Washington Department of Ecology, 2017.
- 334 (5) Feng, X.; Li, Q.; Zhu, Y.; Hou, J.; Jin, L.; Wang, J. Artificial Neural Networks Forecasting
335 of PM_{2.5} Pollution Using Air Mass Trajectory Based Geographic Model and Wavelet
336 Transformation. *Atmospheric Environment* **2015**, *107*, 118–128.
337 <https://doi.org/10.1016/j.atmosenv.2015.02.030>.
- 338 (6) Freeman, B. S.; Taylor, G.; Gharabaghi, B.; Thé, J. Forecasting Air Quality Time Series
339 Using Deep Learning. *Journal of the Air & Waste Management Association* **2018**, *68* (8), 866–
340 886. <https://doi.org/10.1080/10962247.2018.1459956>.
- 341 (7) Zamani Joharestani, M.; Cao, C.; Ni, X.; Bashir, B.; Talebiesfandarani, S. PM_{2.5}
342 Prediction Based on Random Forest, XGBoost, and Deep Learning Using Multisource Remote
343 Sensing Data. *Atmosphere* **2019**, *10* (7), 373. <https://doi.org/10.3390/atmos10070373>.

- 344 (8) Delavar, M.; Gholami, A.; Shiran, G.; Rashidi, Y.; Nakhaeizadeh, G.; Fedra, K.; Hatefi
345 Afshar, S. A Novel Method for Improving Air Pollution Prediction Based on Machine Learning
346 Approaches: A Case Study Applied to the Capital City of Tehran. *ISPRS International Journal of*
347 *Geo-Information* **2019**, 8 (2), 99. <https://doi.org/10.3390/ijgi8020099>.
- 348 (9) Watson, G. L.; Telesca, D.; Reid, C. E.; Pfister, G. G.; Jerrett, M. Machine Learning
349 Models Accurately Predict Ozone Exposure during Wildfire Events. *Environmental Pollution*
350 **2019**, 254, 112792. <https://doi.org/10.1016/j.envpol.2019.06.088>.
- 351 (10) Zheng, Y.; Liu, F.; Hsieh, H.-P. U-Air: When Urban Air Quality Inference Meets Big Data.
352 In *Proceedings of the 19th ACM SIGKDD international conference on Knowledge discovery and*
353 *data mining - KDD '13*; ACM Press: Chicago, Illinois, USA, 2013; p 1436.
354 <https://doi.org/10.1145/2487575.2488188>.
- 355 (11) Pernak, R.; Alvarado, M.; Lonsdale, C.; Mountain, M.; Hegarty, J.; Nehr Korn, T.
356 Forecasting Surface O₃ in Texas Urban Areas Using Random Forest and Generalized Additive
357 Models. *Aerosol Air Qual. Res.* **2019**, 9 (12), 2815–2826.
358 <https://doi.org/10.4209/aaqr.2018.12.0464>.
- 359 (12) Rybarczyk, Y.; Zalakeviciute, R. Machine Learning Approaches for Outdoor Air Quality
360 Modelling: A Systematic Review. *Applied Sciences* **2018**, 8 (12), 2570.
361 <https://doi.org/10.3390/app8122570>.
- 362 (13) Yu, R.; Yang, Y.; Yang, L.; Han, G.; Move, O. RAQ–A Random Forest Approach for
363 Predicting Air Quality in Urban Sensing Systems. *Sensors* **2016**, 16 (1), 86.
364 <https://doi.org/10.3390/s16010086>.

- 365 (14) Zhan, Y.; Luo, Y.; Deng, X.; Grieneisen, M. L.; Zhang, M.; Di, B. Spatiotemporal
366 Prediction of Daily Ambient Ozone Levels across China Using Random Forest for Human
367 Exposure Assessment. *Environmental Pollution* **2018**, *233*, 464–473.
368 <https://doi.org/10.1016/j.envpol.2017.10.029>.
- 369 (15) Breiman, L. Random Forests. *Machine Learning* **2001**, *45* (1), 5–32.
370 <https://doi.org/10.1023/A:1010933404324>.
- 371 (16) Kam, H. T. Random Decision Forest. In *Proceedings of the 3rd International Conference*
372 *on Document Analysis and Recognition*; 1995; Vol. 1416, p 278282.
- 373 (17) Mitchell, T. M. *Machine Learning*; McGraw-Hill series in computer science; McGraw-
374 Hill: New York, 1997.
- 375 (18) Arganis, M. L.; Val, R.; Dominguez, R.; Rodriguez, K.; Dolz, J.; Eato, J. M. Comparison
376 Between Equations Obtained by Means of Multiple Linear Regression and Genetic Programming
377 to Approach Measured Climatic Data in a River. In *Genetic Programming - New Approaches and*
378 *Successful Applications*; Ventura Soto, S., Ed.; InTech, 2012. <https://doi.org/10.5772/50556>.
- 379 (19) Chaloulakou, A.; Assimacopoulos, D.; Lekkas, T. Forecasting Daily Maximum Ozone
380 Concentrations in the Athens Basin. 16.
- 381 (20) Moustris, K. P.; Nastos, P. T.; Larissi, I. K.; Paliatsos, A. G. Application of Multiple Linear
382 Regression Models and Artificial Neural Networks on the Surface Ozone Forecast in the Greater
383 Athens Area, Greece. *Advances in Meteorology* **2012**, *2012*, 1–8.
384 <https://doi.org/10.1155/2012/894714>.

385 (21) Sousa, S.; Martins, F.; Alvimferraz, M.; Pereira, M. Multiple Linear Regression and
386 Artificial Neural Networks Based on Principal Components to Predict Ozone Concentrations.
387 *Environmental Modelling & Software* **2007**, 22 (1), 97–103.
388 <https://doi.org/10.1016/j.envsoft.2005.12.002>.

389 (22) Yuchi, W.; Gombojav, E.; Boldbaatar, B.; Galsuren, J.; Enkhmaa, S.; Beejin, B.; Naidan,
390 G.; Ochir, C.; Legtseg, B.; Byambaa, T.; Barn, P.; Henderson, S. B.; Janes, C. R.; Lanphear, B. P.;
391 McCandless, L. C.; Takaro, T. K.; Venners, S. A.; Webster, G. M.; Allen, R. W. Evaluation of
392 Random Forest Regression and Multiple Linear Regression for Predicting Indoor Fine Particulate
393 Matter Concentrations in a Highly Polluted City. *Environmental Pollution* **2019**, 245, 746–753.
394 <https://doi.org/10.1016/j.envpol.2018.11.034>.

395 (23) Weaver, C. P.; Liang, X.-Z.; Zhu, J.; Adams, P. J.; Amar, P.; Avise, J.; Caughey, M.; Chen,
396 J.; Cohen, R. C.; Cooter, E.; Dawson, J. P.; Gilliam, R.; Gilliland, A.; Goldstein, A. H.; Grambsch,
397 A.; Grano, D.; Guenther, A.; Gustafson, W. I.; Harley, R. A.; He, S.; Hemming, B.; Hogrefe, C.;
398 Huang, H.-C.; Hunt, S. W.; Jacob, D. J.; Kinney, P. L.; Kunkel, K.; Lamarque, J.-F.; Lamb, B.;
399 Larkin, N. K.; Leung, L. R.; Liao, K.-J.; Lin, J.-T.; Lynn, B. H.; Manomaiphiboon, K.; Mass, C.;
400 McKenzie, D.; Mickley, L. J.; O’neill, S. M.; Nolte, C.; Pandis, S. N.; Racherla, P. N.; Rosenzweig,
401 C.; Russell, A. G.; Salathé, E.; Steiner, A. L.; Tagaris, E.; Tao, Z.; Tonse, S.; Wiedinmyer, C.;
402 Williams, A.; Winner, D. A.; Woo, J.-H.; Wu, S.; Wuebbles, D. J. A Preliminary Synthesis of
403 Modeled Climate Change Impacts on U.S. Regional Ozone Concentrations. *Bull. Amer. Meteor.*
404 *Soc.* **2009**, 90 (12), 1843–1864. <https://doi.org/10.1175/2009BAMS2568.1>.

- 405 (24) Gong, X.; Kaulfus, A.; Nair, U.; Jaffe, D. A. Quantifying O₃ Impacts in Urban Areas Due
406 to Wildfires Using a Generalized Additive Model. *Environ. Sci. Technol.* **2017**, *51* (22), 13216–
407 13223. <https://doi.org/10.1021/acs.est.7b03130>.
- 408 (25) Mass, C. F.; Albright, M.; Ovens, D.; Steed, R.; Maciver, M.; Gritmit, E.; Eckel, T.; Lamb,
409 B.; Vaughan, J.; Westrick, K.; Storck, P.; Colman, B.; Hill, C.; Maykut, N.; Gilroy, M.; Ferguson,
410 S. A.; Yetter, J.; Sierchio, J. M.; Bowman, C.; Stender, R.; Wilson, R.; Brown, W. Regional
411 Environmental Prediction Over the Pacific Northwest. *Bull. Amer. Meteor. Soc.* **2003**, *84* (10),
412 1353–1366. <https://doi.org/10.1175/BAMS-84-10-1353>.
- 413 (26) Pacific Northwest Environmental Forecasts and Observations
414 <https://a.atmos.washington.edu/mm5rt/> (accessed Mar 6, 2020).
- 415 (27) Haixiang, G.; Yijing, L.; Shang, J.; Mingyun, G.; Yuanyue, H.; Bing, G. Learning from
416 Class-Imbalanced Data: Review of Methods and Applications. *Expert Systems with Applications*
417 **2017**, *73*, 220–239. <https://doi.org/10.1016/j.eswa.2016.12.035>.
- 418 (28) Jiang, N.; Riley, M. L. Exploring the Utility of the Random Forest Method for Forecasting
419 Ozone Pollution in SYDNEY. **2015**, *1* (5), 10.
- 420 (29) Ukkonen, P.; Manzato, A.; Mäkelä, A. Evaluation of Thunderstorm Predictors for Finland
421 Using Reanalyses and Neural Networks. *J. Appl. Meteor. Climatol.* **2017**, *56* (8), 2335–2352.
422 <https://doi.org/10.1175/JAMC-D-16-0361.1>.
- 423 (30) Jolliffe, I. T.; Stephenson, D. B. *Forecast Verification: A Practitioner's Guide in*
424 *Atmospheric Science*; John Wiley & Sons, 2012.

- 425 (31) Wilks, D. S. *Statistical Methods in the Atmospheric Sciences*; Academic press, 2011; Vol.
426 100.
- 427 (32) Doswell III, C. A.; Davies-Jones, R.; Keller, D. L. On Summary Measures of Skill in Rare
428 Event Forecasting Based on Contingency Tables. *Weather and Forecasting* **1990**, 5 (4), 576–585.
- 429 (33) Murphy, K. P. *Machine Learning: A Probabilistic Perspective*; MIT press, 2012.
- 430 (34) Raschka, S. Model Evaluation, Model Selection, and Algorithm Selection in Machine
431 Learning. *arXiv:1811.12808 [cs, stat]* **2018**.
- 432 (35) Falessi, D.; Narayana, L.; Thai, J. F.; Turhan, B. Preserving Order of Data When Validating
433 Defect Prediction Models. 20.